

CO₂ conversion to CO by fluidized bed biomass gasification: Analysis of operational parameters

Florian J. Müller^{a,*}, Josef Fuchs^{a,2}, Miguel Fanjul Cuesta^{b,3}, Ana Oblanca Gutiérrez^{b,4}, Simon Pratschner^{a,5}, Stefan Müller^{a,6}, Franz Winter^{a,7}

^a Technische Universität Wien, Faculty of Technical Chemistry, Institute of Chemical, Environmental and Bioscience Engineering, Getreidemarkt 9/166, Vienna 1060, Austria

^b ArcelorMittal Global R&D Spain, Avenida de Marqués de Suanes s/n, P.O. Box 90, 33400, Avilés, Asturias, Spain

ARTICLE INFO

Keywords:

CO₂ Conversion
Carbon Capture and Utilization
CCU
Gasification
Fluidized Bed
Biomass

ABSTRACT

Thermochemical conversion of CO₂ with biomass to CO in fluidized bed gasifiers is promising for a sustainable carbon economy. Knowledge about this process is expanded by investigating experimental parameters influencing CO₂ conversion in such a system and combining them to demonstrate effective conversion. Wood char and CO₂ are fed to a lab-scale gasifier in 53 semi-continuous experiments. Six experimental parameters are varied: temperature, bed material type, initial bed-to-fuel ratio, initial fuel loading in the reactor, feed CO₂ flow rate, and fuel particle size. The results are compiled in a semi-empirical model based on reaction kinetics. High temperatures and high fuel-gas contact times are favorable for increasing CO₂ conversion, with the latter achieved through high initial fuel loadings in the reactor and low feed gas flow rates. Choosing olivine instead of silica sand as a bed material also results in higher CO₂ conversions. The highest CO₂ conversion demonstrated in this paper is 86.1%. This experiment produces a gas with 82.75% CO, 10.01% H₂, and 5.90% CO₂ (nitrogen-free and dry).

1. Introduction

1.1. Carbon capture and utilization by biomass CO₂ gasification

The chemical industry accounts for 6.3% of global direct and indirect greenhouse gas emissions (2019) [1]. Two of the most effective strategies to decrease the industry's net emissions by 2030 are defossilizing feedstocks and increasing energy and material efficiency [1]. A limited number of molecules serve as synthesis starting points in this sector. One of these molecules is carbon monoxide, which is used as feedstock for producing various bulk chemicals, e.g., methanol, aldehydes, and alcohols [2]. In 2021, less than 1% of global methanol production was bio-methanol or e-methanol, meaning that most carbon monoxide for

methanol production was derived from natural gas or coal [2,3]. The production and use of methanol accounts for about 0.3 Gt CO₂ emissions per year, about 10% of the total chemical sector emissions [3]. Therefore, defossilizing the production of CO holds vast potential for reducing global greenhouse gas emissions from the chemical industry sector, especially when combined with low-emission hydrogen. This study experimentally investigates how biomass gasification with CO₂ as a gasification agent can be used as carbon capture and utilization (CCU) technology for producing a CO-rich gas from renewable resources.

While gasification in a CO₂ atmosphere has been investigated extensively [4], many studies on CO₂ gasification have neglected the efficient utilization of CO₂ as a feedstock and only considered the conversion of solid materials as a design goal, e.g., [5] or [6]. This work aims to increase the material efficiency of this process by optimizing the

* Corresponding author.

E-mail address: florian.johann.mueller@tuwien.ac.at (F.J. Müller).

¹ <https://orcid.org/0000-0002-8041-2317>

² <https://orcid.org/0000-0002-4627-4475>

³ <https://orcid.org/0009-0008-8256-1106>

⁴ <https://orcid.org/0009-0007-9493-4478>

⁵ <https://orcid.org/0000-0001-6167-586X>

⁶ <https://orcid.org/0000-0001-8878-429X>

⁷ <https://orcid.org/0000-0001-9854-3836>

<https://doi.org/10.1016/j.jcou.2024.102706>

Received 22 May 2023; Received in revised form 13 February 2024; Accepted 13 February 2024

Available online 21 February 2024

2212-9820/© 2024 The Authors. Published by Elsevier Ltd. This is an open access article under the CC BY license (<http://creativecommons.org/licenses/by/4.0/>).

Nomenclature	
$\%_{XCO_2}$	Percentage points CO ₂ conversion, mol/mol.
A	Cross-section of the reactor, m ² .
Ar	Archimedes number, -
B	Initial bed-to-fuel ratio, m ³ /m ³ .
c_A	Dry-based volumetric concentration of the species A, m ³ /m ³ .
d_p	Particle size (weighted average by sieving), m.
$d_{p,n,average}$	Average of mesh sizes on the n th and (n-1) th sieve, m.
d_{SV}	Sauter diameter, m.
E_a	Activation energy, J/mol.
F	Initial fuel loading, m.
f_{umf}	Factor from \dot{V}_{mf} to G , -
g	Gravity of Earth (9.81 m/s ²), m/s ² .
G	Feed gas flow rate, Nm ³ /s.
k	Reaction rate constant, 1/s.
k_0	Preexponential factor, m ^{γ-1} /s (final model... 1/s).
M	Fitting parameter for bed material type, -
m_0	Total mass of sample in the sieving analysis, kg.
m_n	Mass retained on the n th sieve after sieving analysis, kg.
S	Fitting parameter for fuel size, -
t	Reaction time, s.
T	Temperature, K.
T_0	Standard temperature (273.15 K), K.
u_{mf}	Minimum fluidization velocity, m/s.
V	Reactive volume, m ³ .
\dot{V}	Volume flow rate, m ³ /s.
\dot{V}_{mf}	Minimum fluidization flow rate, m ³ /s.
$vol\%_{db}$	Volume percentage, dry-based, m ³ /m ³ .
$vol\%_{db,N_2-free}$	Volume percentage, dry-based, Nitrogen is excluded and other gases are scaled to 100%, m ³ /m ³ .
w_n	Mass fraction of total sample mass retained on the n th sieve after sieving analysis, kg/kg.
X_{CO_2}	CO ₂ conversion, mol/mol.
Δp	Pressure drop in the reactor, mbar.
α	Fitting parameter for B , -
β	Fitting parameter for G , -
γ	Fitting parameter for F , -
ϵ	Assumed bed void fraction of bubbling bed mixture (0.5 m ³ /m ³), m ³ /m ³ .
μ	Dynamic viscosity (fluid), N*s/m ² .
ρ_F	Density (fluid), kg/m ³ .
ρ_P	Density (particle), kg/m ³ .
Φ	Particle sphericity, -
τ	Hydrodynamic residence time, s.
τ_{FGC}	Fuel-gas contact time, s.
Abbreviation, Term	
BECCS	Bioenergy with Carbon Capture, and Storage.
BET	Brunauer-Emmett-Teller (absorption).
CCU	Carbon Capture and Utilization.
DAC	Direct Air Capture.
NDIR	Non-Disperse InfraRed.
PSR	Perfectly Stirred Reactor.
RMSE	Root Mean Square Error.

utilization of CO₂ as a carbon source. Efficient conversion of CO₂ directly lowers carbon dioxide emissions from the process and can save energy by reducing the need for recirculation loops or gas upgrading steps to meet feedstock specifications of downstream units. CO₂ is proposed to come from renewable carbon sources like bioenergy carbon capture and storage (BECCS) or direct air capture (DAC). As the current availability of CO₂ from BECCS is limited, and the cost of CO₂ from DAC is reported at 300–600 \$/ton [3], more efficiently using CO₂ can bring economic benefits. Furthermore, sustainable biomass price and availability are common limitations when scaling up biomass processes to an industrial level [7]. Higher utilization of CO₂ as a carbon source allows more CO to be produced from the same biomass resources, increasing how much conventional fossil production can be replaced.

Among various design options, fluidized bed reactors show key advantages in uniformity of temperature distribution, fuel flexibility, mass and energy transfer rates, and scalability [8]. The design of gasifiers is highly empiric, with a distinct lack of fundamental data on selecting the best process parameters, leading to less than optimal energy and material efficiencies [8]. The current study aims to solve these issues by systematically investigating design parameters and their importance in fluidized bed gasifiers to convert CO₂ to CO. These design parameters are then combined experimentally and in a semi-empirical model to describe and demonstrate the effective utilization of CO₂ as a feedstock.

1.2. State of the art on CO₂ conversion efficiency in gasification

This chapter is used to list how efficiently previous works by other authors have converted CO₂ in allothermal fluidized bed reactors. Experimental parameters are identified from the literature that can help utilize CO₂ as a feedstock more efficiently.

Gasification processes are chemically complex and have the solid

Table 1
Basic heterogeneous and homogenous reactions in CO₂ gasification; adjusted from [15].

Reaction	ΔH_r° (25 °C) in kJ/mol	Reaction name
Basic gas-solid (heterogeneous) reactions		
$C + CO_2 = 2CO$	+173	Boudouard (1)
$C + H_2O = CO + H_2$	+131	Steam-carbon (also water-gas) (2)
$C + 2H_2 = CH_4$	-75	Methanation (3)
$C + (1/2)O_2 = CO$	-111	Partial oxidation of char (4)
Basic gas-gas (homogeneous) reactions		
$CO + H_2O = CO_2 + H_2$	-41	Water-gas shift (5)
$CO_2 + H_2 = CO + H_2O$	+41	Reverse water-gas shift (6)
$CO + (1/2)O_2 = CO_2$	-283	Oxidation of CO (7)
$H_2 + (1/2)O_2 = H_2O$	-242	Oxidation of H ₂ (8)
Decomposition reactions of organic components		
$C_xH_y + xCO_2 = 2xC O + (y/2)H_2$	Endothermic	Dry reforming (9)
$C_xH_y + xH_2O = xCO + (y/2 + x)H_2$	Endothermic	Steam reforming (10)
$C_xH_y + (2x - y/2)H_2 = xCH_4$	Exothermic	Hydrocracking (11)
$C_xH_y + CO_2 = C_{x-1}H_{y-2} + 2CO + H_2$	Endothermic	Dry dealkylation (12)
$C_xH_y + H_2O = C_{x-1}H_{y-2} + CO + 2H_2$	Endothermic	Steam dealkylation (13)
$C_xH_y + H_2 = C_{x-1}H_{y-2} + CH_4$	Exothermic	Hydrodealkylation (14)

carbonaceous feedstock undergoing multiple conversion steps. Many publications provide an overview of gasification in general and CO₂ gasification more precisely [8–10]. The most important reactions for CO₂ gasification are given below in Table 1. The reactions directly converting CO₂ are the Boudouard (Eq. 1), reverse water-gas shift (Eq. 6), dry reforming (Eq. 9), and dry dealkylation (Eq. 12) reactions. Many publications identify the Boudouard reaction as the dominant reaction in the presence of CO₂ as gasification agent, e.g., [11–14].

The CO₂ conversion X_{CO_2} states how much CO₂ fed to the reactor is converted to other carbonaceous molecules. This value is inconsistently described in the literature, usually due to one of two reasons. First, many studies focus on the conversion of solid feedstock in a CO₂ atmosphere and do not describe the conversion of CO₂ in detail [16–19]. Second, inconsistent assumptions and calculation methods are used to evaluate the CO₂ conversion X_{CO_2} , negatively impacting comparability. One example of these differences is the consideration of CO₂ released from biomass during gasification. Some authors consider CO₂ released from biomass pyrolysis in comparable experiments under an N₂ atmosphere to be a separate CO₂ stream entering the reactor [20]. Others only compare ingoing and outgoing CO₂ streams without this pyrolysis credit [21]. This difference in calculation can lead to vastly different results when assessing the same data. Another example of varying calculation methods producing different results is given by [22], which investigates the CO₂ conversion for the same experiment using two methods. In this case, the difference is not if credit for CO₂ from biomass is given, but which: The CO₂ conversion is estimated at 26% using pyrolysis data or 45% using steam gasification data as a reference for the CO₂ produced from biomass.

Both identified problems of a) lacking investigation of the CO₂ conversion X_{CO_2} and b) inconsistent calculation in the literature are solved by reproducing X_{CO_2} from literature instead of directly giving the described values. This reproduction is done by applying a standardized calculation method to available data in the literature. The calculation is based only on the measured product gas composition and does not give credit for CO₂ from pyrolysis. It is described in more detail in the methodology Section 2.3 and used for assessing experiments conducted as part of this paper. Therefore, the CO₂ conversions presented in the results section of this paper can also be directly compared to previous results from other authors given in Table 2. To further ensure comparability, the summary of literature results lists only experimental research on allothermal CO₂ gasification in a fluidized bed. The table lists important parameters describing the process and identifies which correlations with X_{CO_2} were found. The experiment with the highest X_{CO_2} is shown if multiple experiments are described.

The literature given in Table 2 identifies two parameters as potentially increasing CO₂ conversion during gasification in a fluidized bed reactor without co-feeding H₂O. Increasing temperature is commonly associated with higher conversions of biomass and CO₂ in such a system [12,22,25]. Decreasing the ratio of CO₂ to solid carbonaceous material is reported to be another option to increase the relative amount of

converted CO₂ [24]. This ratio can be lowered either by lowering the amount of CO₂ fed to the reactor or by increasing the amount of fuel in the reactor. The highest value for X_{CO_2} in allothermal fluidized bed reactors given in Table 2 is 35%. To the authors' best knowledge, no higher CO₂ conversions have been demonstrated in allothermal fluidized bed reactors.

A comprehensive overview of parameters generally influencing CO₂ gasification processes is available in review papers [9,10]. Although these reviews lack CO₂ conversion data availability and comparability, two more aspects are selected for experimental consideration in this current work. First, the type of bed material is an essential factor in such a system because it can act as a catalyst to promote several reactions. Practical experience shows that for a given bed material, adjusting the ratio of fuel to bed material is also necessary for maintaining stable operation. Second, the size of fuel particles was also varied based on reported significance for mass and heat transfer limitations [10].

Based on the presented previous works, six parameters are selected for experimental investigation on increasing the CO₂ conversion in an allothermal fluidized bed reactor. The six chosen parameters are

- Temperature T ,
- initial fuel loading of the reactor F ,
- fuel particle size S ,
- feed CO₂ gas flow rate G ,
- bed material type M , and
- initial bed-to-fuel volumetric ratio B .

2. Materials and methods

2.1. Materials

Air (dry, compressed), CO₂ (99.995%), and N₂ (99.999%) are supplied to the feeding line with rotameters. Wood char derived from Eucalyptus globulus and prepared by pyrolysis at 700 °C for 20 minutes is used as fuel. The char particles range in size between 0 – 15 mm. Three classes of particles were extracted from this mixture by sieving for experiments investigating the influence of fuel particle size. The range given for the size of the particles refers to the mesh size of sieves used in the separation process. The three classes of fuel size are large fuel (5 – 8 mm), medium fuel (2.5 – 5 mm), and small fuel (0.8 – 2.5 mm). Fuel is fed to the reactor using a screw feeder. In the case of experiments with defined particle size, the screw feeder is bypassed to avoid changing the particle size by abrasion. Proximate analysis is done following these standards: DIN 51718:2002–06 Method A for water content, EN ISO 18122:2015–11 for ash content, and EN ISO 18123:2015–11 for volatile content. Ultimate analysis of this wood char is performed using an Elementar Analyzer EA 1108 CHNS-O by Carlo Erba. An Axios advanced XRF device by Panalytical Analysis gives information on the ash content. Morphological information on the char was gathered by BET (Brunauer-Emmett-Teller) adsorption measurements with N₂ and CO₂ using a

Table 2

Comparison of CO₂ gasification in allothermal fluidized bed reactors in the literature. CO₂ conversion X_{CO_2} is reproduced (rep.) from literature data on product gas composition using Eq. 15 (described in methodology). Atm...Atmospheric pressure.

Fuel vol% CO ₂ Balance=N ₂	Gasification agent °C	Bed material bara	Temperature %	Pressure	X_{CO_2} rep.	X_{CO_2} increased by	Source
Wood sawdust	100	SiC	850	1.5	21	No trend observed	[23] Rep. Fig.6
Wood sawdust	9	Silica sand	934 (700–934)	atm.	17	↑Temperature	[12] Rep. Fig.7
Spent coffee grounds	15 (15–30)	Not given	900	atm.	13	↓CO ₂ :C H ₂ O:CO ₂ synergy	[24] Rep. Fig.8
Lignite	100	Silica sand	850 (850–950)	atm.	35	↑Temperature	[25] Rep. Fig.4
Softwood	100	Olivine	837 (740–840)	atm.	24	↑Temperature	[22] Rep. Fig.8

Table 3
Analysis of Eucalyptus globulus derived wood char used as fuel.

Eucalyptus globulus char			
Proximate and ultimate analysis			
		On dry basis	As received
Water content	wt%	-	6.33
Ash content	wt%	6.28	5.88
Carbon content	wt%	85.42	80.01
Hydrogen content	wt%	1.98	1.86
Nitrogen content	wt%	0.24	0.23
Sulfur content	wt%	<0.02	<0.02
Chlorine content	wt%	0.03	0.03
Oxygen content (by balance)	wt%	6.03	5.64
Volatile matter content	wt%	15.06	14.11
Gross calorific value	kJ/kg	30956	28996
Net calorific value	kJ/kg	30521	28433
Morphological analysis by adsorption of CO ₂			
	N ₂		
Specific surface area (BET)	m ² /g	593	676
Total pore volume	cm ³ /g	0.24	0.34
Average pore diameter	nm	1.6	2.0
Ash melting analysis			
Deformation temperature	°C	1340	
Hemisphere temperature	°C	>1500	
Flow temperature	°C	>1500	
Ash composition			
CaO	wt%	53.0	
K ₂ O	wt%	14.0	
SiO ₂	wt%	7.8	
MgO	wt%	7.1	
Fe ₂ O ₃	wt%	3.8	
P ₂ O ₅	wt%	3.7	
Al ₂ O ₃	wt%	2.8	
Na ₂ O	wt%	2.5	
MnO	wt%	1.7	
SO ₃	wt%	1.6	
Rest	wt%	2.0	

BELSORP-max II by Microtrac. This information is given in (Table 3).

Limestone, silica sand, and olivine are investigated in this paper as bed materials to act as fluidization matrices and potential catalysts. Limestone is expected to undergo thermal composition to quicklime before experiments are started based on the reactor's temperature between experiments (900 °C+) and atmosphere (air and N₂) [26]. These

bed materials are compared in sixteen experiments. Olivine, with a chemical composition of 48–50 wt% MgO, 39–42 wt% SiO₂, and 8.0–10.5 wt% Fe₂O₃, is further used in the remaining 37 experiments investigating other parameters. Due to the small particle size, these bed materials are fluidized at lower gas flow rates. For this reason, they form the bubbling bed fluidization matrix in the reactor, where the fuel is suspended. More detailed explanations and calculations on the fluidization of used materials and the selection of feed gas flow rates are available in Appendix A. The materials used in this investigation are presented in Fig. 1.

2.2. Experimental setup

An electrically heated fluidized bed reactor with a nominal fuel input power of 2 kW_{th} is used in semi-continuous operation. Its general layout is presented in Fig. 2.

The reactor is made from stainless steel (X15CrNiSi25–21), has an inner diameter of 53.1 mm, and has two main zones connected by a flange. The supplied gas is nearly pure CO₂ with a small stream of N₂ (<1%), which is necessary for purging the pressure measurement. CO₂ enters the reactor's lowest point and flows towards the off-gas line. The first zone the gas enters is the preheating zone, which is heated by two half-shell heating shells. These half-shells are rated at a nominal power of 0.75 kW_{el} and are 250 mm high. They are made from ceramic fiber and can heat up to 900 °C. The preheated gas then flows towards a sieve tray, where the flow is distributed. The reaction zone is also heated by two identical half-shell heating shells, which can heat up to 1000 °C. These temperature limitations refer to the highest possible set points for the heating shells on the reactor's outside. The temperatures observed inside the reactor are lower due to static heat losses. The off-gas stream from the reactor is a mixture of product gas, entrained particles, and minor impurities such as tar. This mixture is conditioned for measurement by a two-step particle separation and drying in Impinger bottles at –2 °C.

The dry gas stream is fed to an Emerson Rosemount NGA 2000 continuous gas measuring device. This device can measure CO₂, CO, H₂, and CH₄ between 0% and 100% and O₂ up to 25%. CO₂, CO, H₂, and CH₄ are measured by non-disperse infrared (NDIR), while O₂ is measured paramagnetically. The accuracy is ±1% of the calibrated maxima,

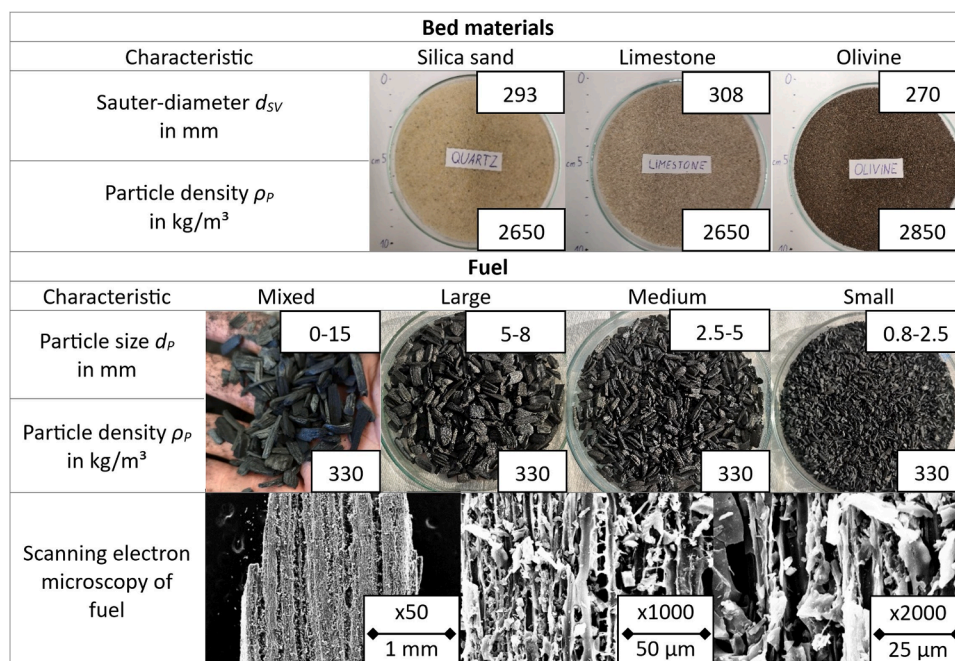


Fig. 1. Materials used in described experiments.

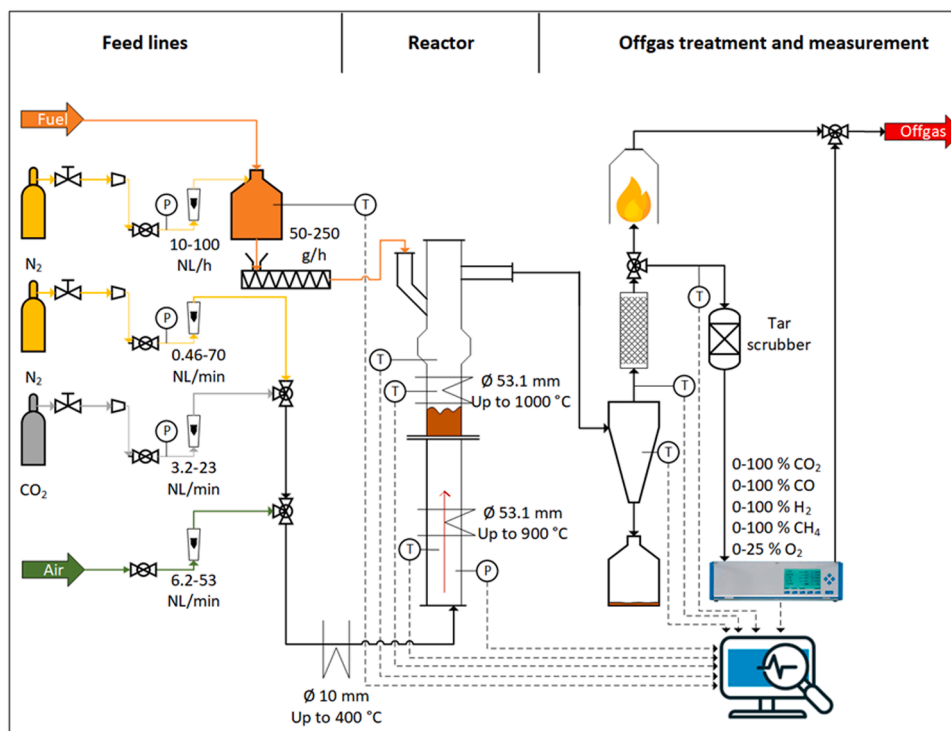


Fig. 2. Electrically heated fluidized bed reactor.

which are given in Appendix B. These accuracies were used to obtain the error ranges in Section 3.1. Further measurements include temperature measurements by thermocouples type K and a pressure measurement below the sieve tray. The temperature measurement used as the reference for this paper's investigations is centered in the reaction zone.

Semi-continuous experiments, as defined by Missen et al. [27], with a batch of initially inserted wood char and continuous feeding of CO₂ and removal of product gas are used to determine the CO₂ conversion within this paper. This type of experiment is favored over experiments using continuous fuel feed to increase the speed of the investigation and overcome reactor limitations from insufficient heating power. CO₂ conversion is assessed close to the experiment's start when biomass conversion is still low, and wood char is available in excess (differential reactor). A more detailed explanation of the experimental procedure is given in Appendix B.

In total, 53 experiments are performed in this reactor (Fig. 2) to assess the influence of six parameters on CO₂ conversion. Parameters are varied in isolation and combined to determine their impact on X_{CO_2} . A summary of investigated settings is given in Table 4. A complete list of experiments can be found in Appendix C.

Table 4
Experimental parameters investigated within this work.

Abbreviation	Investigated factor	Operational parameters (target values)	Variations
<i>T</i>	Temperature	800 – 1000 °C	5
<i>F</i>	Initial fuel loading (height)	5 – 15 cm	4
<i>S</i>	Fuel size	0.8 – 8 mm	4
<i>G</i>	Feed gas flow rate	0.30 – 0.43 Nm ³ /h	2
<i>M</i>	Bed material type	Silica sand limestone olivine	3
<i>B</i>	Initial bed-to-fuel ratio	0.66 – 4 m ³ /m ³	6

2.3. Calculation of CO₂ conversion

The CO₂ conversion is evaluated in this work by applying a calculation method using the dry-based volumetric concentrations of the product gas components CO, CO₂, and H₂, which are expressed as c_A , where A is the molecule species. Using this method, X_{CO_2} can be calculated continuously with a matching resolution of one second as the gas measurement. The equation for this method is given by [28] and considers the Boudouard (Eq. 1) and steam-carbon (Eq. 2) reactions. It assesses how much educt CO₂ is converted to product CO by the Boudouard reaction. This calculation is corrected for any CO instead produced by the steam-carbon reaction, which also produces H₂.

$$X_{CO_2} = \frac{c_{CO} - c_{H_2}}{c_{CO} - c_{H_2} + 2 \cdot c_{CO_2}} \quad (15)$$

Eq. 15 describes the CO₂ conversion X_{CO_2} , which aims to describe the change in mass of CO₂ before and after the reactor. This equation is used to evaluate all experiments conducted in the scope of this paper. Reference [28] does not provide context for the applicability of this equation. The following assumptions are considered to apply:

- No CO or H₂ is present in the feed gas. This assumption is most valid for feedstocks like char and coal, which have relatively limited volatile content and do not contribute significantly to the gas composition via devolatilization. With increasing volatile content, the uncertainty of the calculation can increase.
- Solid carbon is only converted to gas via reactions in Eq. 1 to Eq. 3. This assumption also faces increasing uncertainty from increasing volatile content in biomass.

The fuel used in this study has low volatile and oxygen contents. Furthermore, fuel is fed into the hot reactor under a nitrogen atmosphere shortly before the gasification starts. Data show some gaseous pyrolysis products are released when fuel is fed into the hot nitrogen atmosphere, but minimal devolatilization products are measured at the gasification start (Appendix B). For these reasons, the assumptions

described above are considered to apply, which lowers the uncertainty in calculating X_{CO_2} .

The X_{CO_2} data presented in the results section are the average value of a 10–14 second period near the start of gasification (Appendix B). This methodology is chosen because this period represents the maximum observed CO₂ conversion before the conversion drops due to temperature and fuel decreases. An average value over this short period is used instead of only the data point with maximum conversion to reduce noise from relying on a single data point. The error ranges of figures in Section 3.1 result from the uncertainty in gas concentration measurement.

2.4. Semi-empirical CO₂ conversion model development

Correlations between the six investigated parameters and the CO₂ conversion are reported in the experimental Section 3.1. These empirical results are combined and conceptualized in the modeling part of this paper in a semi-empirical model based on simplified reaction kinetics. The proposed model replicates the CO₂ conversion in the investigated bubbling bed reactor based only on the described parameters and excludes or generalizes phenomena for which data are unavailable, e.g., bed expansion and bubble formation. After simplification, this model can approximate the CO₂ conversion in this allothermal fluidized bed reactor based on a small set of process characteristics.

The thermodynamic equilibrium of this chemical system in the investigated temperature range is calculated using FactSage. This calculation suggests high CO₂ conversions of 78.7% at 800 °C to 98.3% at 1000 °C in equilibrium. The observed experimental CO₂ conversions are generally significantly lower and suggest a rate-controlled system behavior, indicating X_{CO_2} should be described as a function of the reaction time t . Fluidized bed reactors' essential advantage is their heat and material distribution uniformity. For this reason, the model is proposed using the hydrodynamic residence time distribution of a perfectly stirred reactor (PSR). For a first-order reaction in a PSR, the literature suggests Eq. 16 to describe the CO₂ conversion [29].

$$X_{CO_2} = \int_0^{\infty} [1 - \exp(-k \cdot t)] \cdot \frac{1}{\tau} \exp\left(-\frac{t}{\tau}\right) dt = \frac{k \cdot \tau}{1 + k \cdot \tau} \quad (16)$$

The simplified form of this equation eliminates the reaction time t and describes the conversion of CO₂ using the reaction rate constant k and the hydrodynamic residence time τ . The hydrodynamic residence time τ describes the average time of CO₂ in the reactor as the ratio of reactive volume V and volume flow rate \dot{V} (Eq. 17). Since this investigation is heavily focused on solid-gas reactions, the reactive volume is assumed as the volume taken by the fuel-bed material mixture. For this reason, the feed gas flow rate (G), given at the standard temperature T_0 , is corrected to reactor temperature T and combined with the cross-section of the reactor (A), initial fuel loading (F), initial bed material-to-fuel ratio (B), and bed void fraction of mixed bed (ε) to calculate τ . The bed void fraction and height during gasification are not available from this experimental setup. Bed void fractions between 0.4 and 0.6 are reported for binary bed material and biomass mixtures in bubbling fluidized beds, e.g., in [30–32]. In this work, an estimation of 0.5 for the mixed bed void fraction ε is used for all experiments. The height of the bed material-fuel mixture is described in two terms to assess two aspects individually: initial fuel loading (F) in an otherwise empty reactor and added bed material ($1+B$).

$$\tau = \frac{V}{\dot{V}} \rightarrow \tau = \frac{A \cdot F \cdot (1+B) \cdot \varepsilon}{G \cdot T / T_0} \quad (17)$$

The reaction rate constant k describes the rate and direction of the reaction. k can be explained by the Arrhenius expression, which represents the temperature and activation energy E_a dependency of k (Eq. 18). The preexponential factor k_0 summarizes various effects, e.g., the likelihood of reaction species collision, and is used as a fitting parameter.

The exponential term represents the fraction of collisions with enough energy to overcome the activation energy barrier. Initial fuel loading (F) and fuel size (S) in the reactor are proposed to be correlated with available reaction sites and, therefore, the preexponential factor. The potential catalytic activity of bed material is associated with changes in activation energy, which the variable M expresses.

$$k = k_0 \cdot \exp\left(\frac{-E_a}{R \cdot T}\right) \rightarrow \quad (18)$$

$$k = k_0 \cdot S \cdot F \cdot \exp\left(\frac{-E_a \cdot M}{R \cdot T}\right)$$

Initial bed-to-fuel ratio (B), feed gas flow rate (G), temperature (T), and initial fuel loading (F) are available as quantified values for each experiment and are plugged into the model in SI units. Exponential scaling factors α , β and γ are used to scale these values to investigate their relative influence while achieving the best fit. M and S are not available as representative quantified values and are therefore left as dimensionless variables to solve. Bed material influence is considered using the dimensionless variable M , which describes the scaling of activation energy as a function of bed material type. M has one value for all experiments with silica sand and another value for all experiments with olivine as a bed material. Limestone is not included in this model since its reactions with CO₂ go beyond catalytic activity, so the calculated CO₂ conversion is not comparable within the same model. Fuel size is a complex parameter with a multifactorial influence. Morphological particle characteristics like specific surface area and pore size directly influence heat and mass transport. Particle size also affects X_{CO_2} indirectly by stabilizing the bubbling bed fluidization regime at smaller particle sizes, leading to a more homogenous heat and material distribution. These varying correlations make values like the mean particle size an unsuitable scaling factor. A dimensionless variable S with four discrete values for the four size classes analogous to the procedure for bed material types is used as a way around this issue. The combined modeling expression is given by Eq. 19.

$$X_{CO_2} = \frac{k_0 \cdot S \cdot \exp\left(\frac{-E_a \cdot M}{R \cdot T}\right) \cdot \frac{A \cdot F \cdot (1+B) \cdot \varepsilon}{(G \cdot T / T_0)^\beta}}{1 + k_0 \cdot S \cdot \exp\left(\frac{-E_a \cdot M}{R \cdot T}\right) \cdot \frac{A \cdot F \cdot (1+B) \cdot \varepsilon}{(G \cdot T / T_0)^\beta}} \quad (19)$$

3. Results

Experimental data are presented in this chapter to describe the influence of individual parameters on CO₂ conversion. The data presented here aim to explain the trends in CO₂ conversion due to parameter variation. At the end of this chapter in Section 3.2, a semi-empirical model combining the individual investigations is proposed. This model describes which parameters can be selected to reach this fluidized bed reactor's highest CO₂ conversion.

3.1. Influence of experimental parameters on the CO₂ conversion

3.1.1. Temperature

To assess the influence of temperature on the CO₂ conversion, the reactor's electrical heating was operated at set points between 800 and 1000 °C. The measured temperature in the reaction zone during the evaluation period is used for all evaluations. The materials used for these experiments are 5 cm of wood char (16.9 g) and 10 cm of olivine. CO₂ feed gas flow rate is 0.43 Nm³/h, around ten times the minimum fluidization velocity u_{mf} at 1200 K. Fig. 3a shows the evolution of X_{CO_2} over the gasification duration, while Fig. 3b compares X_{CO_2} at the time of evaluation.

Increasing the temperature strongly enhances the CO₂ conversion in the investigated interval. X_{CO_2} increases from 11.9% at 803.0 °C to 48.7% at 981.5 °C. Equilibrium conditions for this system were

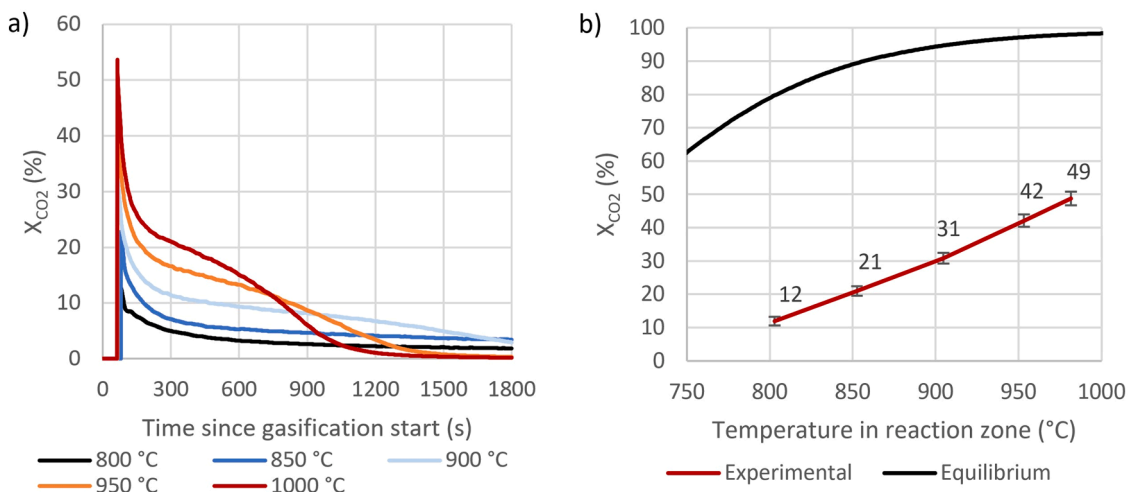


Fig. 3. a) X_{CO_2} over the time of gasification (temperature given is the set point temperature; measured values differ). b) Influence of temperature on X_{CO_2} at various temperatures (temperature measured). Thermodynamic equilibrium is calculated using FactSage.

calculated using FactSage and are dominated by the Boudouard reaction (Eq. 1). Thermodynamic equilibrium suggests a much smaller relative increase from about 80% X_{CO_2} to 98% in the same temperature range. Therefore, the experimentally observed X_{CO_2} is significantly closer to equilibrium at higher temperatures. These data align with literature finding CO₂ char gasification to be the rate-limiting step of the global pyro-gasification reaction with a duration near 95% of the entire biomass conversion time [6]. Different rate-controlled regimes and increased reaction speeds at higher temperatures are reported [18]. In summary, this experimental data and FactSage calculation support that increasing the temperature is crucial for increasing CO production in thermodynamic equilibrium and lowering the reaction time necessary to reach equilibrium.

3.1.2. Fuel loading in the reactor

Fig. 4 compares X_{CO_2} for a range of initial fuel loadings in the reactor, given as the initial height at the experiment start. Experiments are performed at 1000 °C and 900 °C set point temperature with 10 cm of olivine as bed material in the reactor. The CO₂ feed gas flow rate is set to 0.30 or 0.43 Nm³/h, which equals seven or ten times the minimum gas flow rate for fluidization of the bed material particles.

The reactor's initial fuel amount significantly correlates with the CO₂

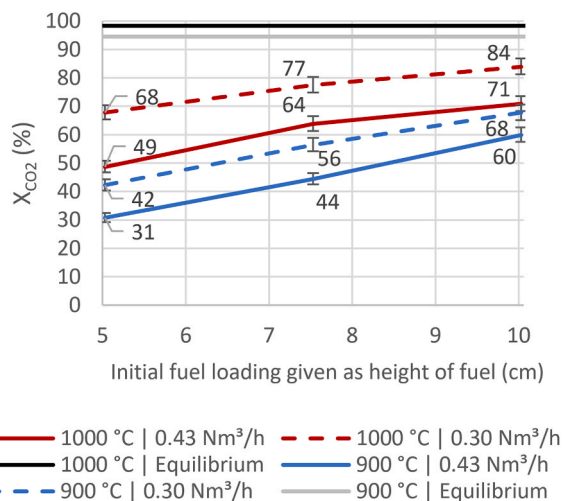


Fig. 4. Influence of initial fuel loading (given as initial height in the reactor at experiment start in cm) and feed gas flow rate (CO₂ superficial flow rate) on CO₂ conversion X_{CO_2} . Thermodynamic equilibrium is calculated using FactSage.

conversion in these experiments. An increase from 67.8% to 83.9% for X_{CO_2} is achieved by increasing initial fuel loading in the reactor from 5 cm (16.9 g) to 10 cm (33.9 g) at 1000 °C (set point). At the time of these evaluations, shortly after the experiments started, solid material was available in excess during all experiments, and only a negligible amount of fuel had been converted. Therefore, this increased CO₂ conversion is a result of increasing the contact time of CO₂ with the fluidized bed. The contact time of feed CO₂ flowing with 0.3 Nm³/h in the mixture of olivine and wood char is increased from 0.42 s at 5 cm initial fuel loading to 0.56 s at 10 cm initial fuel loading for an assumed bed void fraction ϵ of 0.5 at 1000 °C. Calculating the gas-fuel contact time by disregarding the bed material and only considering the wood char in the reactor would result in a linear correlation between the contact time and the initial fuel loading in the reactor. For this assumption, doubling the fuel loading from 5 cm to 10 cm also doubles the gas-solid contact time from 0.14 s to 0.28 s.

The positive correlation between more fuel in the reactor and higher X_{CO_2} values is also underpinned by the decline of X_{CO_2} observed after the evaluated period. Fig. 3a shows a significant reduction of X_{CO_2} over half an hour of gasification. Temperature set points, CO₂ feed gas flow rates, and bed material are constant, but the initially batch-fed fuel is used up and not replaced. While the sharp decline in X_{CO_2} at the beginning is most likely due to endothermic reactions lowering the temperature in the reactive zone, X_{CO_2} trends towards zero when the fuel amount in the reactor decreases. The CO₂ conversion approaches zero once the fuel is converted, which happens faster at higher temperatures with higher CO₂ conversion and, therefore, fuel conversion via the Boudouard reaction. This trend supports the finding that X_{CO_2} is higher with higher amounts of fuel in the reactor and higher fuel-gas contact time.

3.1.3. Fuel particle size

Three classes of wood char size were extracted from the mixed-size fuel by sieving. The three classes of fuel size are large fuel (5 – 8 mm), medium fuel (2.5 – 5 mm), and small fuel (0.8 – 2.5 mm). Fig. 5 shows CO₂ conversions as measured for these three classes of particles and the mixed-size fuel at various initial fuel loading values. The set point temperature for all depicted experiments is 1000 °C. The feed gas flow rate is 0.30 Nm³/h, equivalent to seven times the minimum number necessary for fluidizing the bed material at 1200 K. Olivine is placed 10 cm high in the reactor as bed material for all experiments.

The CO₂ conversion efficiency increase observed with increasing initial fuel loading holds for all investigated fuel particle classes. At 5–10 cm fuel heights, there is little difference in performance between small, medium, and mixed-size wood char particles used as fuel. Large

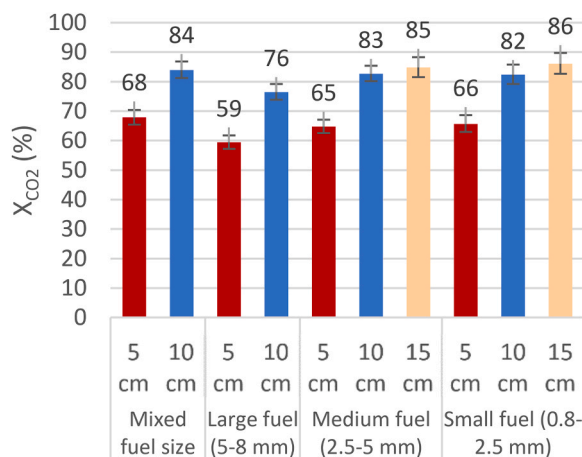


Fig. 5. Influence of fuel particle size at various initial fuel loadings (given as initial height in the reactor at experiment start in cm) on CO₂ conversion X_{CO_2} .

fuel particles (5–8 mm) show lower CO₂ conversions at 5 cm (59.4% vs. average 66.1%) and 10 cm initial fuel loading (76.5% vs. average 83.0%). A possible explanation is given by higher specific surface area and better heat and mass transfer in smaller particles [33,34]. In addition, an inhibition effect resulting from increased CO concentration in the particles' pores is reported to be more significant for larger particles [35]. These data suggest that this system might have a threshold fuel particle size, which sees larger fuel particles showing lower X_{CO_2} .

Several authors report an increase in mixing quality when smaller biomass [36,37] or coal [38,39] particles are fluidized in smaller bed material particles. Fluidization calculations in Appendix A indicate that the lower X_{CO_2} value observed for large fuel particles might be connected with the fluidization of fuel particles. The calculation shows that the applied feed gas flow rate leads to a superficial gas velocity that exceeds the minimum fluidization velocity u_{mf} of small wood char particles and is close to u_{mf} for medium-sized wood char. In contrast, the calculated minimal fluidization velocity for large wood char particles is not reached. Appendix D also shows differences observed for gasification experiments with small and medium fuel particles at high fuel loadings extended after the evaluation period.

3.1.4. Feed gas flow rate

The CO₂ conversion as a function of the gas flow rate of CO₂ fed to the reactor is compared in Fig. 4 for various initial fuel loadings and temperatures.

Increased feed gas flow rates are correlated with lower X_{CO_2} at all temperatures and initial fuel loadings. Decreasing the CO₂ superficial flow rate from 0.43 Nm³/h to 0.30 Nm³/h increases the fuel-gas contact time by 41.1%. On average, X_{CO_2} is increased by 26.1% due to this, again suggesting a strong correlation between fuel-CO₂ contact time and X_{CO_2} . This observation is consistent with all investigated parameter combinations. It can be concluded that decreasing the feed gas flow rate increases X_{CO_2} by increasing the fuel-gas contact time. At a flowrate of zero and infinite gas-solid contact time, the thermodynamic equilibrium limits this increase. For fluidized bed reactors, another practical limit is given by the minimal flow rate necessary for fluidization (Appendix A).

3.1.5. Bed material type

Fig. 6 compares three bed materials described in Fig. 1 under identical conditions. The reactor's electrical heating is operated at set points between 800 and 1000 °C. The materials used for these experiments are 5 cm of wood char (16.9 g) and 10 cm of each bed material. CO₂ feed gas flow rate is 0.43 Nm³/h.

Comparing silica sand and olivine as bed material reveals a clear improvement in CO₂ conversion for using olivine over silica sand. At the

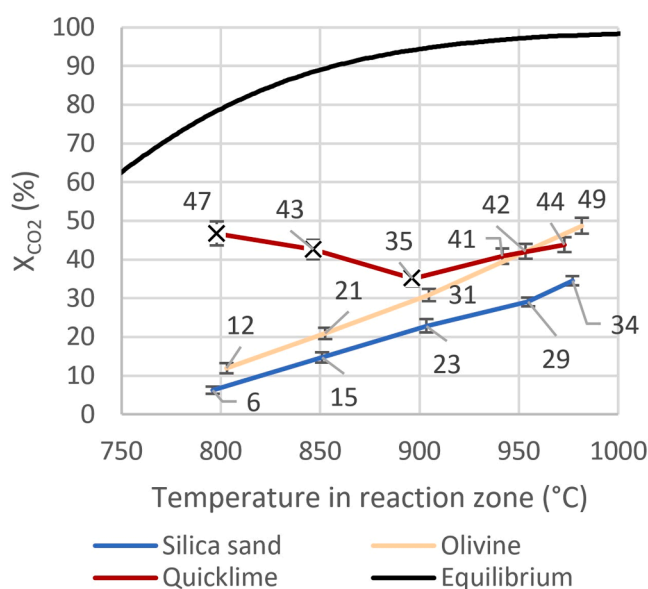


Fig. 6. Influence of bed material type on X_{CO_2} at various temperatures (temperature is measured). Thermodynamic equilibrium is calculated using FactSage. Data marked with X are an artifact resulting from quicklime binding CO₂.

highest investigated set point temperature of 1000 °C, a reactor containing silica sand converts CO₂ at 34.5%, while olivine exhibits a CO₂ conversion of 48.7%.

Limestone is showing significantly higher CO₂ conversions at temperatures below 950 °C. Carbon balancing around the reactor and comparing temperature changes at the beginning of gasification reveals this to be an artifact resulting from quicklime capturing CO₂. Before every experiment, the reactor is conditioned by burning leftover fuel with air at 1000 °C and adjusting the set point temperature under a nitrogen atmosphere. These conditions favor the production of quicklime, which is the expected compound at the experiment start [26]. Up to 900 °C, the exothermic carbonation reaction of quicklime binding CO₂ and forming limestone is expected. The overestimated CO₂ conversions under these conditions result from removing unconverted CO₂ from the produced gas. This effect removes the comparability of the generated data from using limestone with other bed materials in this study, as indicated in Fig. 6. At higher temperatures, these data suggest conversion efficiency similar to olivine, but the trendline increases less steeply. Due to the carbonation reaction phasing out over increased temperature, these data are too inconclusive and restricted to estimate the effect of limestone as a bed material on CO₂ conversion with sufficient confidence.

3.1.6. Bed-to-fuel ratio

Variations of the initial volumetric bed-to-fuel ratio are compared by keeping the same amount of wood char in the reactor and varying only the amount of olivine used as bed material. This variation is performed to see if the longer gas-solid contact time with the olivine-wood char mixture resulting from increased bed height would increase the CO₂ conversion. If olivine catalyzes the conversion of CO₂, e.g., via the Boudouard reaction, another effect of increasing this ratio could be a more pronounced catalytic effect. Fig. 7 shows the results of this investigation, which was performed using 5 cm of wood char loaded into the reactor. Set point temperatures are varied between 900 and 1000 °C. The feed gas flow rate is 0.30 Nm³/h, equivalent to seven times the minimum number necessary for fluidizing the bed material at 1200 K.

Increasing the initial bed-to-fuel ratio B by 50% by adding more olivine increases X_{CO_2} by only 0.8% on average. Doubling B lowers the observed X_{CO_2} by 6.1% on average. The experimental error ranges obtained for these experiments are 3.6–5.4% in CO₂ conversion. This

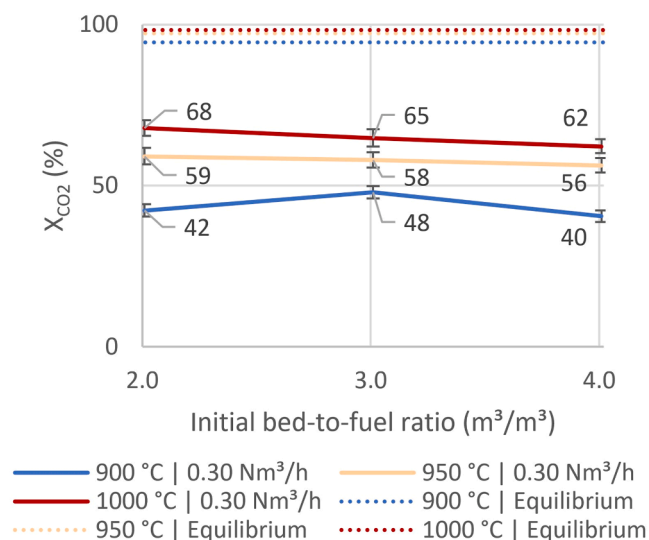


Fig. 7. Influence of initial volumetric bed-to-fuel ratio on X_{CO_2} at various parameters (temperature is set point) for olivine as bed material. Thermodynamic equilibrium is calculated using FactSage.

inconclusive trend, minor overall changes, and error ranges suggest the influence of B on CO_2 conversion efficiency to be negligible.

The stability of the bubbling fluidized bed in continuous operation is an effect not consistently represented by the calculation method for CO_2 conversions in this paper. Appendix D describes how differences in fluidization could explain lower X_{CO_2} values during prolonged investigation, using Figure D-1 as an example.

3.2. CO_2 conversion model

The 53 experimental results presented in Section 3.1 are plugged into the theoretical CO_2 conversion model (Eq. 19). First, X_{CO_2} is calculated for each experiment using a placeholder value of 1 for α , β , γ , M , S , k_0 , and E_a . The root square error between the modeled and observed X_{CO_2} is calculated for each experiment. The sum of errors is divided by 53 to calculate the root mean square error (RMSE), which describes the model's accuracy in estimating the measured CO_2 conversions. Second, the variables α , β , γ , M , S , k_0 , and E_a are solved by Excel Solver, minimizing the root mean square error (RMSE). M for olivine and S for mixed-size fuel are kept at the initial value of 1 for comparability. Third, one by one, the scaling factors are excluded from the model to check if their exclusion significantly increases RMSE, lowering model quality. Excluding parameters from the model lowers its flexibility and increases RMSE to increase model simplicity and focus on the most important identified parameters. A parameter is deemed significant here if its exclusion from the model increases RMSE by more than 1% $_{X_{CO_2}}$. The remaining parameters and solved variables are proposed as a semi-empirical model able to predict CO_2 conversion in this gasification system (Table 5).

The proposed model simplifies the hydrodynamic residence time term τ (Eq. 17) to a new time descriptor termed fuel-gas contact time τ_{FGC} . This simplification results from the modeling suggesting no correlation between the amount of bed material and the conversion of CO_2 in the reactor. The new term τ_{FGC} describes a hypothetical reactor with the same initial fuel loading F and bed void fraction ϵ as the real fluidized bed reactor but without any bed material (Eq. 20).

$$\tau_{FGC} = \frac{A \cdot F \cdot \epsilon}{G \cdot T / T_0} \quad (20)$$

Nearly no increase in RMSE is observed after eliminating the initial bed-to-fuel ratio B from the model by setting α to 0 and only considering the gas flow rate G as a linear factor in calculating τ_{FGC} by changing β to

the value 1. Eliminating the fuel size S as a parameter increases RMSE by around 0.19% $_{X_{CO_2}}$. Further simplification of the model increases RMSE by 0.63% $_{X_{CO_2}}$ when the initial fuel loading F is also only considered as a linear factor in the calculation of τ_{FGC} by changing γ to the value 1. Eliminating the bed material parameter M increases RMSE by more than 1% $_{X_{CO_2}}$ and is therefore not done. The simplified model uses only T , M , and τ_{FGC} (formed using F and G) as parameters and approximates the experimental data at an RMSE value of 4.06% $_{X_{CO_2}}$. This value lies within the error ranges obtained from experimental data due to the uncertainty in gas concentration data. The experimental data shows error ranges between 1.3% and 7.1% $_{X_{CO_2}}$.

The temperature in the reactor has a strong influence on X_{CO_2} in the final model. Higher temperatures decrease the time to approach equilibrium by increasing the reaction rate constant k according to the Arrhenius equation (Eq. 18). Higher temperatures also favor CO production via the Boudouard reaction (Eq. 1) in equilibrium. For a fuel-gas contact time of 0.25 seconds and olivine as bed material, the model predicts the CO_2 conversion to increase from 26% at 800 °C to 80% at 1000 °C.

The initial fuel loading in the reactor and the feed gas flow rate are combined to form the fuel-gas contact time (Eq. 20), significantly influencing the CO_2 conversion in the final model. A correlation between time and conversion is expected for all chemical systems which are not in thermodynamic equilibrium. This aspect of the model solution is confirmed by comparing the observed CO_2 conversions versus the higher conversions suggested by the thermodynamic equilibrium calculation using FactSage. For a temperature of 1000 °C and olivine as bed material, the model predicts the CO_2 conversion to increase from 67% at 0.125 seconds to 80% at 0.25 seconds of fuel-gas contact time.

The activation energy E_a decreases by around 6% if the bed material is switched from silica sand to olivine. This decrease in activation energy increases X_{CO_2} at all investigated temperatures, thus making olivine a better choice of bed material in CO_2 gasification. Without a baseline for the investigated system given by experiments that use neither silica sand nor olivine, this study does not answer if either bed material catalyzes the conversion of CO_2 . The relative difference could be explained by olivine acting as a catalyst or silica sand as an inhibitor in this model. An alkali index reported in the literature, which evaluates the catalytic activity of ash in coal or char, supports both explanations [40]. Silicon, the main component in silica sand, is suggested to act as an inhibitor if it is part of the ash [40]. Magnesium and iron comprise around 60 wt% of olivine and are reported elsewhere to show moderate catalytic in the fuel matrix [10] or if mixed with the fuel as a powder. The low correlation between the bed-to-fuel ratio and X_{CO_2} given by the model suggests that olivine might not be catalytically active.

The activation energy identified in this model is around 139 kJ/mol for olivine as a bed material. This value agrees with the literature, which identifies four reaction domains in CO_2 gasification. For thermogravimetric analyzers, free-fall fixed-bed reactors, and drop-tube reactors, activation energies of 125–147 kJ/mol are reported in the temperature range of 900–1000 °C, and the system is characterized as particle or bed diffusion-controlled [18]. The same authors identify no diffusion limitation for a fluidized bed reactor but report a sharp decrease of activation energy at 1250 K from chemical-controlled 232 kJ/mol to a system-specific external mass transfer limitation. Other sources do not investigate different limitation regimes but agree with the broad range of activation energy (141–160 kJ/mol given by [41]) or find higher activation energies around ~250 kJ/mol, which is likely due to lower temperatures resulting in a chemically controlled system [18,42]. In summary, the activation energy found in this work generally agrees well with the literature data, giving credibility to the underlying model (Table 5).

The simplified model is depicted in Fig. 8, which uses olivine and silica sand as bed materials in two viewpoints each. The tips of the arrows represent experimentally found X_{CO_2} . The colored lattice is the model approximation of these values, and the transparent lattice is the

Table 5

Modeling parameters for designing a semi-empirical CO₂ conversion model in the described fluidized bed gasifier; 1*...Set as 1 for comparability.

Parameter	Full model	Simplified model
Model equation	Eq. 19	$X_{CO_2} = \frac{k_0 \cdot \exp\left(\frac{-E_a \cdot M}{R \cdot T}\right) \cdot \tau_{FGC}}{1 + k_0 \cdot \exp\left(\frac{-E_a \cdot M}{R \cdot T}\right) \cdot \tau_{FGC}}$
α	0.036	-
β	1.115	1
γ	1.377	1
Quartz	1.06	1.07
Olivine	1*	1*
Fuel mixed	1*	-
Small fuel	1.008	-
Medium fuel	1.121	-
Large fuel	0.878	-
k_0 in $m^3 \cdot s^{-1}$	4.67E+06	7.95E+06
E_a in J/mol	138800	138800
RMSE in % X_{CO_2}	3.24	4.06

thermodynamic equilibrium for this system, as given by FactSage.

The gap between the thermodynamic equilibrium and the experimental CO₂ conversion decreases with higher temperatures and fuel-gas contact times. The system is closer to equilibrium for using olivine (left) instead of silica sand (right) as a bed material due to the lower observed activation energy using olivine. This model approximation matches the

highest experimentally observed X_{CO_2} . Table 6 and Figure B-1 give information about the experiment using the highest investigated set point temperature and initial fuel loading, the lowest feed gas flow rate, and olivine as a bed material. With these settings, the described experiment operates close to the reactor's geometrical and durability limits to convert 86.1% of CO₂ compared to a model approximation of 83.4%. This conversion vastly exceeds the highest CO₂ conversion previously observed in a similar reactor, reproduced by the same calculation method at 35% (Table 2) [25]. The resulting gas is rich in CO and has an H₂-to-CO ratio of around 1:8. This ratio is too low for direct conversion of the gas to methanol or in Fischer-Tropsch-synthesis, which need an H₂-to-CO ratio of around 2:1 [3,43]. For this reason, the gas needs to be enriched in H₂ to be used as a synthesis gas, e.g., by adding hydrogen from water electrolysis.

4. Conclusion

The influence of experimental parameters on CO₂ conversion in an allothermal fluidized bed reactor is described in this paper. Positive correlations are identified and combined to increase the conversion of CO₂. The investigated parameters are process characteristics, and the results can be used for highly efficient reactor design. The 53 semi-continuous experiments described in this work are performed in a fluidized bed reactor with a nominal power of 2 kW_{th}. A parameter variation including the six parameters temperature (T), bed material type

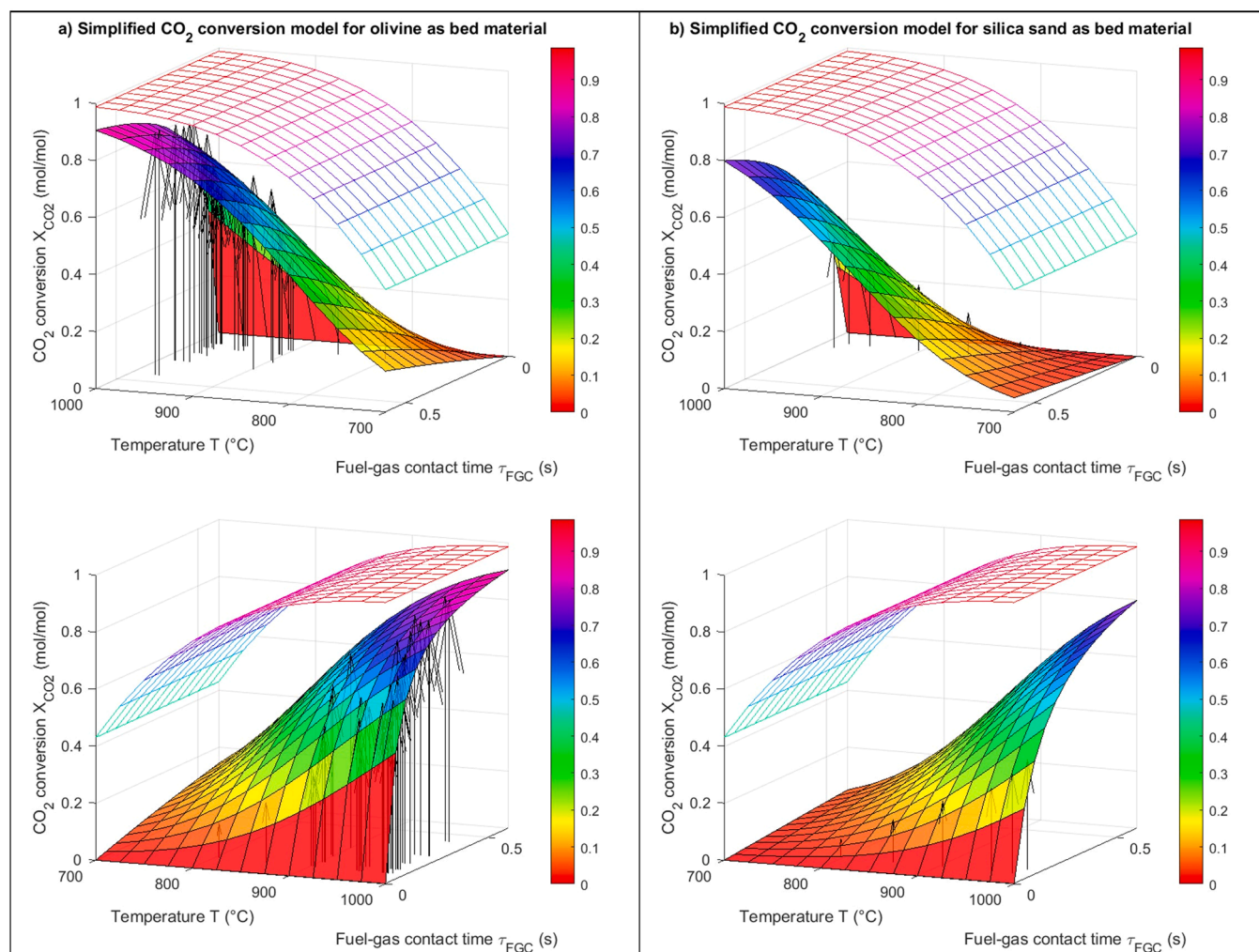


Fig. 8. Simplified semi-empirical CO₂ conversion model (filled lattice), thermodynamic equilibrium (empty lattice), and experimentally observed values (arrow tips) for CO₂ conversion. A) Olivine as bed material, and b) silica sand as bed material.

Table 6

Comparison of model approximation and experimental data on the experiment with the highest CO₂ conversion X_{CO_2} in this paper.

Experiment #53		Operational parameters						
Temperature (set point) °C	Temperature (measured) °C	Initial fuel loading cm	Feed gas flow rate Nm ³ /h	Bed material -	Initial bed-to-fuel-ratio m ³ /m ³	Fuel size mm		
1000	970	15	0.30	Olivine	0.67	0.8–2.5		
Average data during evaluation period								
CO vol% _{db,N2-free}	CO ₂ vol% _{db,N2-free}	CH ₄ vol% _{db,N2-free}	H ₂ vol% _{db,N2-free}	Rest vol% _{db,N2-free}	X_{CO_2} experimental %	X_{CO_2} model %		
82.75	5.90	0.05	10.01	1.30	86.1	83.4		

(M), initial bed-to-fuel ratio (B), initial fuel loading in the reactor (F), feed gas flow rate (G), and particle size (S) is conducted. (Table 4) The main results of this study are:

- CO₂ gasification in a fluidized bed is demonstrated to convert CO₂ to CO at very high rates. The highest conversion observed within this publication is 86.1%, producing gas with 82.75% CO, 10.01% H₂, and only 5.90% CO₂. (Table 6)
- This system's experimentally observed CO₂ conversion can be replicated in a semi-empirical model based on reaction kinetics with a root mean square error of 4.06% X_{CO_2} . The calculated activation energy of 139 kJ/mol matches well with the literature. (Table 5)
- The CO₂ conversion in the investigated system can be effectively increased by using higher temperatures, higher initial fuel loading in the reactor, lower feed gas flow rates, and olivine instead of silica sand as a bed material. The fuel loading and feed gas flow rate can be combined as the newly defined fuel-gas contact time τ_{FGC} (Eq. 20). No clear correlation was observed between X_{CO_2} and a change in bed-to-fuel ratio or fuel particle size. (Fig. 8)
- Although fuel size and bed-to-fuel ratio are not observed to strongly influence X_{CO_2} in the system, they are to be considered for the stability of the bubbling bed fluidization regime. Unstable fluidization from too low a bed-to-fuel ratio might also decrease X_{CO_2} . This effect can be countered by lowering fuel particle size to promote their direct fluidization. (Figure D-1)

In summary, this work highlights the importance of multiple parameters for efficiently converting the greenhouse gas CO₂ with biomass to product gas with very high CO content. While increasing temperature is the dominant parameter, this also likely comes with energy penalties in practical applications. Increasing fuel-gas contact time by optimizing reactor design promises a significant increase in X_{CO_2} without increasing the ongoing cost of operation. Larger commercial reactors operated under similar conditions would allow for higher gas-solid contact times, further increasing CO₂ conversion compared to the findings in this study.

Hydrodynamic aspects like bed expansion or bubble formation were not investigated in this work. Experiments were performed with a highly carbonaceous biomass with low volatile content. When using biomass with higher volatile content, the resulting gas could be mixed with devolatilization products and potentially lowered in CO content.

This thermochemical carbon conversion pathway could provide CO-rich gas for multiple green production chains in the chemical industry. Additional hydrogen is necessary for chemical synthesis to meet the hydrogen-to-carbon monoxide ratio demands of common processes, such as methanol production or Fischer-Tropsch synthesis. This hydrogen should be produced by low-emission technologies, e.g., water electrolysis with renewable electricity, to achieve overall emission savings. For industrial applications, it has to be considered that utilizing CO₂ via the Boudouard reaction is highly energy-intensive due to its endothermic nature. Compared to other biomass gasification processes, the high conversion of CO₂ to CO demonstrated in this work means that less carbon monoxide needs to be produced from biomass. Furthermore, a lowered CO₂ content in the produced gas can bring energy savings

from reduced gas separation and recirculation demand. This process can substitute CO from coal or natural gas in synthesizing bulk chemicals like methanol, aldehydes, and alcohols. Therefore, biomass CO₂ gasification as a carbon capture and utilization technology could lower the life cycle emissions from the chemical industry significantly, supposed CO₂ and biomass are sustainably sourced and renewable.

The chemical interactions between fuel and bed materials should be investigated in future studies to improve the understanding of catalytic effects. A numeric simulation study looking into hydrodynamic aspects could provide further insights into the specifics of mass transfer and gas-fuel contact times. Using a water-CO₂ mixture as the gasification agent or using different fuels should be investigated for their potential to increase the hydrogen-to-carbon monoxide ratio in the produced gas. The model proposed within this work should be compared to results obtained from continuous operation at a larger scale and with other fuel types. Special attention needs to be given to energy demands and losses, which are beyond the scope of this study. The technical results should be contextualized in future investigations with life cycle and techno-economic assessments in various production chains.

CRedit authorship contribution statement

Florian J. Müller: Writing – review & editing, Writing – original draft, Visualization, Validation, Software, Methodology, Investigation, Formal analysis, Data curation, Conceptualization, **Josef Fuchs:** Writing – review & editing, Validation, Resources, Project administration, Methodology, Funding acquisition, Conceptualization, **Miguel Fanjul Cuesta:** Writing – review & editing, Validation, Resources, **Ana Oblanca Gutiérrez:** Writing – review & editing, Validation, Resources, **Simon Pratschner:** Writing – review & editing, Visualization, **Stefan Müller:** Writing – review & editing, Supervision, Resources, Project administration, Funding acquisition, Conceptualization, **Franz Winter:** Writing – review & editing, Supervision, Resources, Project administration, Funding acquisition, Conceptualization.

Declaration of Competing Interest

The authors declare that they have no known competing financial interests or personal relationships that could have appeared to influence the work reported in this paper.

Data availability

Data will be made available on request.

Acknowledgments

This study was carried out within the doctoral college CO₂Refinery at TU Wien. This work is also part of the research project CO₂ Reduction for Ironmaking by Utilization of Process Gases, Part 1, and received support from ArcelorMittal Innovación Investigación e Inversión, S.L. Furthermore, the authors would like to thank Microtrac MRB for the characterization of the fuel particle surface. In addition, the authors would like to thank TU Wien Bibliothek for covering article processing charges through its

Open Access Funding program.

Appendix A. Fluidization calculations

The fluidization state of particles is a function of particle and gas characteristics and operating conditions. The following section explains the calculations behind selecting gas flow rates for the bubbling fluidized bed used in this work.

Particle size is determined by sieving analysis. Bed materials were analyzed by a cascade of sieves with mesh sizes from 1 mm to 63 µm. The sieving analysis results and particle size d_p values are given in Table A-1.

Table A-1

Sieving analysis of bed materials. The data reflect the average result for each bed material. Three samples were analyzed per bed material. N.d...Not detected

Bed material g	m_0 µm	Sieve number n µm	Mesh size g	$d_{p,n,average}$ g/g	m_n µm	w_n	$d_p \pm$ standard deviation
Silica sand	448.097	1	1000				366±2.1
		2	400	700	169.883	0.379	
		3	280	340	177.983	0.397	
		4	224	252	61.237	0.137	
		5	180	202	28.653	0.064	
		6	140	160	7.950	0.018	
		7	100	120	2.033	0.005	
		8	63	81.5	0.320	0.001	
		9	0	31.5	0.037	0.000	
Limestone	176.917	1	1000				385±3.5
		2	400	700	122.307	0.691	
		3	280	340	46.953	0.265	
		4	224	252	3.717	0.021	
		5	180	202	1.170	0.007	
		6	140	160	0.310	0.002	
		7	100	120	0.323	0.002	
		8	63	81.5	0.483	0.003	
		9	0	31.5	1.653	0.009	
Olivine	112.497	1	1000				337±0.1
		2	400	700	0.193	0.002	
		3	280	340	109.563	0.974	
		4	224	252	2.603	0.023	
		5	180	202	0.110	0.001	
		6	140	160	0.027	0.000	
		7	100	120	N.d.	N.d.	
		8	63	81.5	N.d.	N.d.	
		9	0	31.5	N.d.	N.d.	

The values are the average data from three analyses, and the standard deviations observed in these analyses for the particle size d_p are noted. Eq A-1 was used to determine the particle size d_p from $d_{p,n,average}$, the average of mesh sizes on the n^{th} and $(n-1)^{\text{th}}$ sieve, and the corresponding weight fraction w_n , which relates the mass retained on the n^{th} sieve m_n to the total sample mass m_0 .

$$d_p = 1 / \sum_{n=2}^9 \frac{m_n}{m_0 \cdot d_{p,n,average}} = 1 / \sum_{n=2}^9 \frac{w_n}{d_{p,n,average}} \quad (\text{A-1})$$

For the experiments comparing the effect of fuel particle size (see Section 3.1.3), four sieves were used to separate the fuel mixture into three classes of particles. Sieves with 8 mm and 0.8 mm mesh sizes were used as upper and lower limits, with larger and smaller particles being discarded. The remaining fuel particles were split into three classes: 0.8 – 2.5 mm (small char), 2.5 – 5.0 mm (medium char), and 5.0 – 8.0 mm (large char) based on the mesh size of sieves used for separation. The resulting bed material and fuel particle sizes are given as d_p in Table A-2 and Table A-3. The particle sphericity Φ is used to relate this particle size d_p to the Sauter-diameter d_{sv} , which is needed for fluidization calculations, see Eq A-2. The sphericity is 1 for ideal spheres. It has a lower limit of 0 for increasingly non-spherical particles. This value is not measured in this work but is taken from literature suggesting a sphericity of 0.76 for average sand particles, which is used for all bed materials [44]. Particle sphericity of wood char from wood chips is also taken from the literature [45]. No particle size change is suggested for calcinating limestone particles of this size at 900 °C [46]. Therefore, the density change from limestone to quicklime closely follows stoichiometric considerations based on the calcination reaction of CaCO_3 . The resulting density of all bed materials, including uncalcined and calcined lime, is taken from an earlier study at TU Wien, which used the same materials [47].

$$d_{sv} = \Phi \cdot d_p \quad (\text{A-2})$$

The minimum fluidization velocity u_{mf} is the superficial gas velocity at which the drag force of the fluidizing gas becomes equal to the gravitational force of the particles. This velocity allows the particles to transition from a fixed bed to a fluidized bed regime. The minimum gas velocity necessary for fluidizing the bed particles is calculated using Eq A-3, as given in the literature [48,49]. Eq A-4 provides the Archimedes number Ar , which introduces the solid density. The ideal gas law is used to calculate gas densities at different temperatures.

$$u_{mf} = \frac{\mu}{\rho_F \cdot d_{sv}} \cdot (\sqrt{33.7^2 + 0.0408 \cdot Ar} - 33.7) \quad (\text{A-3})$$

$$Ar = \frac{\rho_F \cdot d_{sv}^3 \cdot (\rho_P - \rho_F) \cdot g}{\mu^2} \quad (\text{A-4})$$

The results of these calculations are summarized for all bed materials and distinct fuel size classes in [Table A-2](#). Feed gas flow rates are selected as 0.30 and 0.43 Nm³/h to achieve five to ten times u_{mf} of the investigated bed material as superficial gas velocity, expressed as f_{umf} . These values result in a bubbling bed fluidization regime for all three bed materials. Quicklime exceeds this window due to its lower density, but the calculated f_{umf} is still suitable to form a bubbling fluidized bed.

Table A-2

Fluidization properties of all used bed materials at 1200 K and atmospheric pressure.

Variable	Unit	Silica sand	Limestone	Quicklime	Olivine
d_p	m	3.66E-04	3.85E-04	3.85E-04	3.37E-04
Φ	-	7.60E-01 [44]	7.60E-01 [44]	7.60E-01 [44]	7.60E-01 [44]
d_{SV}	m	2.79E-04	2.93E-04	2.93E-04	2.56E-04
ρ_F (1200 K)	kg/m ³	4.34E-01	4.34E-01	4.34E-01	4.34E-01
ρ_P	kg/m ³	2.65E+03 [47]	2.65E+03 [47]	1.50E+03 [47]	2.85E+03 [47]
μ (1200 K)	N*s/m ²	4.68E-05 [50]	4.68E-05 [50]	4.68E-05 [50]	4.68E-05 [50]
g	m/s ²	9.81E+00	9.81E+00	9.81E+00	9.81E+00
Ar	-	1.11E+02	1.29E+02	7.33E+01	9.32E+01
u_{mf}	m/s	2.61E-02	2.88E-02	1.63E-02	2.37E-02
A	m ²	2.21E-03	2.21E-03	2.21E-03	2.21E-03
\dot{V}_{mf}	Nm ³ /h	4.73E-02	5.23E-02	2.96E-02	4.31E-02
f_{umf} (0.30 Nm ³ /h)	-	6.3	5.7	10.1	7.0
f_{umf} (0.43 Nm ³ /h)	-	9.1	8.2	14.5	10.0

The selected flow rates of 0.30 – 0.43 Nm³/h can also be used to calculate f_{umf} for the fuel particles ([Table A-3](#)). The particle density of wood char was determined by water displacement measurement. These calculations result in f_{umf} above 1 for small fuel particles, around 1 for medium-sized particles and below 1 for large particles. The effect of these differences is described and discussed in the main body of this work (see [Section 3.1.3](#)).

Table A-3

Fluidization properties of char used as fuel at 1200 K and atmospheric pressure.

Variable	Unit	Small char	Medium char	Large char
d_p	m	1.65E-03	3.75E-03	6.50E-03
Φ	-	6.60E-01 [45]	6.60E-01 [45]	6.60E-01 [45]
d_{SV}	m	1.09E-03	2.48E-03	4.29E-03
ρ_F (1200 K)	kg/m ³	4.34E-01	4.34E-01	4.34E-01
ρ_P	kg/m ³	3.30E+02	3.30E+02	3.30E+02
μ (1200 K)	N*s/m ²	4.68E-05 [50]	4.68E-05 [50]	4.68E-05 [50]
g	m/s ²	9.81E+00	9.81E+00	9.81E+00
Ar	-	8.28E+02	9.72E+03	5.06E+04
u_{mf}	m/s	4.93E-02	2.37E-01	5.75E-01
A	m ²	2.21E-03	2.21E-03	2.21E-03
\dot{V}_{mf}	Nm ³ /h	8.94E-02	4.30E-01	1.04E+00
f_{umf} (0.30 Nm ³ /h)	-	3.4	0.7	0.3
f_{umf} (0.43 Nm ³ /h)	-	4.8	1.0	0.4

Appendix B. Detailed description of the experimental procedure

Semi-continuous experiments with continuously fed CO₂ and initially inserted wood char are used to determine the CO₂ conversion within this paper. This type of experiment has trade-offs with continuous experiments.

Three advantages can be identified compared to evaluating stationary points in continuous experiments: A first reason, which is essential when assessing so many operational parameters, is the speed of investigation. Semi-continuous experiments are quicker to perform than investigating stable continuous operation points because there is no need to wait for the system to reach its steady state. For this reason, more parameters can be studied in the same amount of time. This advantage is present in many batch or semi-batch experiments.

The other reasons are system-specific and hail from reactor and measurement limitations with the used setup. Second, the conditions at the time of investigation are close to the initial conditions and can thus be relatively accurately known. The fuel amount and size of particles in the reactor change during the gasification process and are not measured in this system. Evaluating only close to the experimental start reduces unknown modifications to the selected parameters. Third, endothermic reactions (see [Table 1](#)) cool the reactor significantly and lower its temperature. Since this system's primary reaction converting CO₂ is the endothermic Boudouard reaction, the cooling effect intensifies with increasing X_{CO_2} . This effect reduces the maximum achievable temperature in the reactor. During comparable continuous experiments, the highest temperatures achieved in this reactor were around 100 °C lower. As a result, semi-continuous experiments can be used to correlate reactor temperature to CO₂ conversion in fluidized bed reactors over a broader range.

Compared to continuous experiments, some disadvantages of this type of experiment are less accurately representing industrial production and

lacking the ability to conduct an energy balance properly. Mid- and long-term effects like catalyst deactivation or the risk of reactor blockage could be assessed better in continuous experiments. Additionally, ongoing fuel feeding would lead to overlapping fuel devolatilization and gasification reactions, which might produce different gas compositions than semi-continuous experiments. While these aspects are not the primary focus of this study, future follow-up works performed with continuous feeding are expected to expand the knowledge compared to the data presented in this paper.

During the experiments conducted in this work, gasification is preceded in the reactor by a short pyrolysis phase, as shown in Figure B-1. During pyrolysis (white background), the reactor is heated and flushed under a nitrogen atmosphere. Fuel is added under the N₂ atmosphere at experimental temperature, leading to small amounts of devolatilization. This phase of devolatilization reduces the influence of the pyrolysis gases on the measured gas composition during gasification, increasing the accuracy of the CO₂ conversion calculation.

In the gasification phase (green), CO₂ replaces N₂ as a fluidization agent. The physical distance between the reaction zone and NDIR measurement induces a delay of 30–60 seconds, which depends on the amounts of gases produced, temperature, and feed gas flow rate. Evaluating close to the starting conditions reduces the uncertainty of fuel loading and fuel size, and also ensures that wood char is available in excess and does not limit the conversion of CO₂ stoichiometrically. To comparably start the evaluation period for all experiments at small fuel conversions, a standardized method to eliminate this delay is applied. The evaluation begins once the sum of carbonaceous components (CO, CO₂, CH₄) in the produced gas exceeds 10 vol %_{db}. This cutoff number is selected because it coincides well with the first observed CO₂ conversion plateau before the conversion starts dropping due to the temperature and fuel decrease. The CO₂ conversion is averaged over 10 s for the higher and 14 s for the lower investigated feed gas flow rate to assess equal amounts of CO₂ fed to the reactor. Concentrations are measured every 1 s, and Eq. 15 is applied each second. Averaging over this short evaluation period means that changes to reactor conditions remain minor, while potential errors in assessing X_{CO₂} resulting from measurement noise are reduced (see Figure B-1). Some nitrogen is in the measured gas throughout the gasification experiment because N₂ is used as an inert gas to flush the fuel hopper and is added to the product gas after the reactor but before measurement.

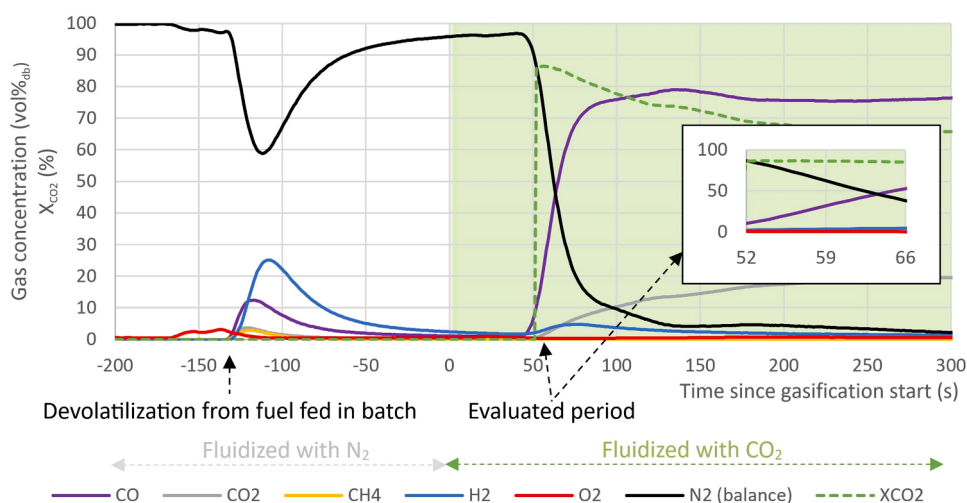


Figure B-1. Experimental procedure in two phases: 1. Fuel is fed at the experimental temperature under N₂ atmosphere (white background). 2. CO₂ replaces N₂ to start gasification (green background). Magnified: Evaluated period for the CO₂ conversion X_{CO₂}. More information on experimental parameters for this experiment is given in Table 6.

Temperatures used in the evaluations are taken at the beginning of gasification since thermocouples do not suffer from the same 30 – 60 seconds delay in measurement. The measured temperatures in the reactor are lower than the heating shells' outside temperature set point due to static heat losses and rapidly cool with increasing CO₂ conversion due to the endothermic reactions. Evaluating the CO₂ conversion as described close to the experimental start minimizes the changes to the reactor temperature resulting from this cooling effect. CO₂ is replaced by air after 30 minutes of gasification to combust residual unconverted coke in the reactor, preparing it for the next experiment. During the combustion phase, the temperature is between 900 – 1000 °C, which is also expected to facilitate a complete decomposition of limestone to quick lime and CO₂. However, with this setup, solid samples are not available during operation; therefore, experimental proof of this decomposition cannot be given.

The equipment used in this study has the following error tolerances:

- Dry gas composition measurement: 1 vol% of calibrated maximum. The calibrated maxima were
 - o 47.1 vol% CO₂
 - o 25.0 vol% CO
 - o 10.1 vol% CH₄
 - o 20.9 vol% O₂
 - o 7.7 vol% H₂
- Temperature measurement by thermocouple type K: 4‰ of measured temperature

Appendix C. List of experiments

Table C-1

Full list of experiments.

Exp. Nr	Fuel	Bed material	Target temperature	CO ₂ feed	Number of new experiments
		height	height	Volume flow	

(continued on next page)

Table C-1 (continued)

Exp. Nr	Fuel	Bed material		Target temperature °C	CO ₂ feed Volume flow NL/min	Number of new experiments	
		height cm	height cm				
1-5	Wood char	5	Silica sand sand	10	800 850 900 950 1000	7.2	5
6	Wood char	5	Silica sand sand	10	1000	5.1	1
7-11	Wood char	5	Limestone	10	800 850 900 950 1000	7.2	5
12-16	Wood char	5	Olivine	10	800 850 900 950 1000	7.2	5
17-22	Wood char	5	Olivine	15 20	900 950 1000	7.2	6
23-31	Wood char	5	Olivine	10 15 20	900 950 1000	5.1	9
32-35	Wood char	7.5 10	Olivine	10	900 1000	7.2	4
36-39	Wood char	7.5 10	Olivine	10	900 1000	5.1	4
40-43	Large wood char 5-8 mm	5 10	Olivine	10	1000	5.1 7.2	4
44-48	Medium wood char 2.5-5 mm	5 10 15	Olivine	10	1000	5.1 7.2	5
49-53	Small wood char 0.8-2.5 mm	5 10 15	Olivine	10	1000	5.1 7.2	5
Total variations	4	3	3	3	5	2	53

Appendix D. Comparison of fluidization and its effect when using high loadings of small- and medium-sized fuel

This section details experimental differences observed when investigating fuel particles with different sizes for a longer duration than the short evaluation period, which is used to calculate and compare X_{CO_2} in this work (Appendix B). For more information about the effect of this parameter on CO₂ conversion observed during the evaluation period, see Section 3.1.3.

Data for experiments with an initial fuel loading of 15 cm are given for medium and small fuel. Figure D-1 compares two experiments conducted at 1000 °C set point temperature and a CO₂ feed gas flow rate of 0.30 Nm³/h. Both investigations use 10 cm olivine as bed material and 15 cm initial fuel loading. The experiments differ in initial parameters only by choice of fuel particle size (medium and small). The data shown in Figure D-1 are recorded several minutes after the evaluated period for comparing X_{CO_2} .

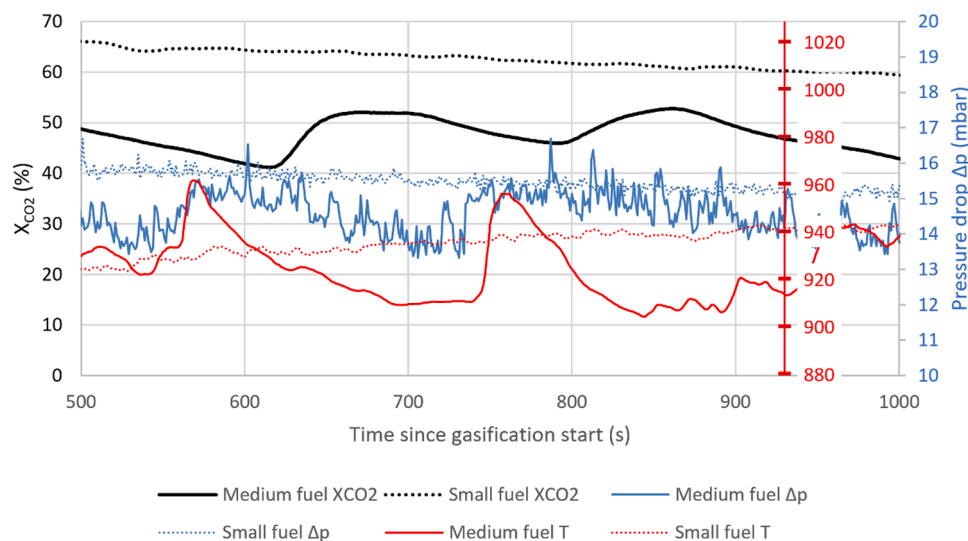


Figure D-1. Comparison of fluidization stability (fluctuations in pressure drop) for medium (2.5 – 5 mm) and small (0.8 – 2.5 mm) fuel particle sizes at 15 cm initial fuel loading; Effect on reaction zone temperature and CO₂ conversion.

Pressure drop measurements across the reactor are shown in Figure D-1 to fluctuate significantly more for medium-sized than for small-sized fuel. This type of fluctuation is uncharacteristic for bubbling fluid bed regimes. Appendix A shows that the superficial gas velocity in these experiments with

0.30 Nm³/h CO₂ feed flow rate is around 3.4 times u_{mf} for small wood char and 0.7 times u_{mf} for medium wood char. Therefore, one explanation could be that the bed for the experiment with medium-sized fuel deviates from bubbling bed behavior due to the fuel particles' u_{mf} value below 1. The temperature spikes shortly after the average pressure drop decreases. This temperature spike can be explained by insufficient mixing when considering the heat source is on the reactor walls while the temperature measurement is in the reactor's core. When mixing is insufficient for efficiently transporting heat from the hot walls to the reactor's core, this lowers the CO₂ conversion. As a result of the decreased heat transport, less energy is available for the endothermic gasification reactions in the reactor. The CO₂ conversion drops at a delay of around 60 seconds, which is explained by the time the gas needs to flow through the measurement line. These data indicate that smaller fuel might facilitate higher CO₂ conversion during continuous operation at high fuel loadings by improving fluidization.

References

- [1] IPCC, *Climate Change 2022 - Mitigation of Climate Change*, Cambridge, 2022, [10.1017/9781009157926](https://doi.org/10.1017/9781009157926).
- [2] 2017/2117 for the production of large volume organic chemicals, 2017. European Commission, Commission Implementing Decision (EU) .
- [3] IRENA and Methanol Institute, "Innovation Outlook: Renewable Methanol," Abu Dhabi, 2021.
- [4] M.F. Irfan, M.R. Usman, K. Kusakabe, Coal gasification in CO₂ atmosphere and its kinetics since 1948: a brief review, *Energy* vol. 36 (1) (2011) 12–40, <https://doi.org/10.1016/j.energy.2010.10.034>.
- [5] R. Liu, Y. Zhang, Z. Ling, Y. Song, Some new insights into the synergy occurring during char gasification in CO₂/H₂O mixtures, *Fuel* vol. 268 (February) (2020) 1–8, <https://doi.org/10.1016/j.fuel.2020.117307>.
- [6] C. Guizani, O. Louissard, F.J.E. Sanz, S. Salvador, Gasification of woody biomass under high heating rate conditions in pure CO₂: experiments and modelling, *Biomass. Bioenergy* vol. 83 (2015) 169–182, <https://doi.org/10.1016/j.biombioe.2015.09.017>.
- [7] V. Lenz, N. Szarka, M. Jordan, D. Thrän, Status and perspectives of biomass use for industrial process heat for industrialized countries, *Chem. Eng. Technol.* vol. 43 (8) (2020) 1469–1484, <https://doi.org/10.1002/ceat.202000077>.
- [8] S. De, A.K. Agarwal, V.S. Moholkar, B. Thallada, *Coal and biomass gasification*, Springer Singapore, 2018, <https://doi.org/10.1007/978-981-10-7335-9>.
- [9] Y.H. Chan, S.N.F. Syed Abdul Rahman, H.M. Lahuri, A. Khalid, Recent progress on CO-rich syngas production via CO₂ gasification of various wastes: a critical review on efficiency, challenges and outlook, *Environ. Pollut.* vol. 278 (2021) 116843, <https://doi.org/10.1016/j.envpol.2021.116843>.
- [10] P. Lahijani, Z.A. Zainal, M. Mohammadi, A.R. Mohamed, Conversion of the greenhouse gas CO₂ to the fuel gas CO via the Boudouard reaction: a review, *Renew. Sustain. Energy Rev.* vol. 41 (2015) 615–632, <https://doi.org/10.1016/j.rser.2014.08.034>.
- [11] X. Yao, Q. Yu, Z. Han, H. Xie, W. Duan, Q. Qin, Kinetics of CO₂ gasification of biomass char in granulated blast furnace slag, *Int. J. Hydrog. Energy* vol. 43 (27) (2018) 12002–12012, <https://doi.org/10.1016/j.ijhydene.2018.04.102>.
- [12] N. Sathwani, S. Adhikari, M.R. Eden, Biomass gasification using carbon dioxide: effect of temperature, CO₂/C ratio, and the study of reactions influencing the process, *Ind. Eng. Chem. Res.* vol. 55 (10) (2016) 2883–2891, <https://doi.org/10.1021/acs.iecr.5b04000>.
- [13] Z. Wang, et al., Towards enhanced catalytic reactivity in CO₂-assisted gasification of polypropylene, *Fuel* vol. 284 (July 2020) (2021) 1–9, <https://doi.org/10.1016/j.fuel.2020.119076>.
- [14] P. Lahijani, M. Mohammadi, Z.A. Zainal, A.R. Mohamed, Advances in CO₂ gasification reactivity of biomass char through utilization of radio frequency irradiation, *Energy* vol. 93 (2015) 976–983, <https://doi.org/10.1016/j.energy.2015.09.092>.
- [15] M. Pohorelý, M. Jeremiáš, K. Svoboda, P. Kameníková, S. Skoblia, Z. Beňo, CO₂ as moderator for biomass gasification, *Fuel* vol. 117 (2014) 198–205, <https://doi.org/10.1016/j.fuel.2013.09.068>.
- [16] S. Tong, L. Li, L. Duan, C. Zhao, E.J. Anthony, A kinetic study on lignite char gasification with CO₂ and H₂O in a fluidized bed reactor, *Appl. Therm. Eng.* vol. 147 (June 2018) (2019) 602–609, <https://doi.org/10.1016/j.applthermaleng.2018.10.113>.
- [17] L. Reyes, L. Abdelouahed, B. Campusano, J.C. Buvat, B. Taouk, Exergetic study of beech wood gasification in fluidized bed reactor using CO₂ or steam as gasification agents, *Fuel Process. Technol.* vol. 213 (July 2020) (2021) 1–12, <https://doi.org/10.1016/j.fuproc.2020.106664>.
- [18] P. Stoesser, C. Schneider, T. Kreitzberg, R. Kneer, T. Kolb, On the influence of different experimental systems on measured heterogeneous gasification kinetics, *Appl. Energy* vol. 211 (October 2017) (2018) 582–589, <https://doi.org/10.1016/j.apenergy.2017.11.037>.
- [19] S. Gül, F. Akgün, E. Aydar, N. Ünlü, Pressurized gasification of lignite in a pilot scale bubbling fluidized bed reactor with air, oxygen, steam and CO₂ agents, *Appl. Therm. Eng.* vol. 130 (2018) 203–210, <https://doi.org/10.1016/j.applthermaleng.2017.11.021>.
- [20] Z. Liu, F. Zhang, H. Liu, F. Ba, S. Yan, J. Hu, Pyrolysis/gasification of pine sawdust biomass briquettes under carbon dioxide atmosphere: Study on carbon dioxide reduction (utilization) and biochar briquettes physicochemical properties, *Bioresour. Technol.* vol. 249 (2018) 983–991, <https://doi.org/10.1016/j.biortech.2017.11.012>.
- [21] Y. Cheng, Z. Thow, C.H. Wang, Biomass gasification with CO₂ in a fluidized bed, *Powder Technol.* vol. 296 (2016) 87–101, <https://doi.org/10.1016/j.powtec.2014.12.041>.
- [22] A.M. Mauerhofer, et al., Conversion of CO₂ during the DFB biomass gasification process, *Biomass. Convers. Biorefin.* vol. 11 (1) (2021) 15–27, <https://doi.org/10.1007/s13399-020-00822-x>.
- [23] S. Valin, L. Bedel, J. Guillaudeau, S. Thiery, S. Ravel, CO₂ as a substitute of steam or inert transport gas in a fluidised bed for biomass gasification, *Fuel* vol. 177 (2016) 288–295, <https://doi.org/10.1016/j.fuel.2016.03.020>.
- [24] H.A. Kibret, Y.L. Kuo, T.Y. Ke, Y.H. Tseng, Gasification of spent coffee grounds in a semi-fluidized bed reactor using steam and CO₂ gasification medium, *J. Taiwan Inst. Chem. Eng.* vol. 119 (2021) 115–127, <https://doi.org/10.1016/j.jtice.2021.01.029>.
- [25] N. Spiegl, X. Long, C. Berruoco, N. Paterson, M. Millan, Oxy-fuel co-gasification of coal and biomass for negative CO₂ emissions, *Fuel* vol. 306 (August) (2021) 1–8, <https://doi.org/10.1016/j.fuel.2021.121671>.
- [26] J. Fuchs, J.C. Schmid, S. Müller, H. Hofbauer, Dual fluidized bed gasification of biomass with selective carbon dioxide removal and limestone as bed material: A review, *Renew. Sustain. Energy Rev.* vol. 107 (June 2019) (2019) 212–231, <https://doi.org/10.1016/j.rser.2019.03.013>.
- [27] R.W. Missen, C.A. Mims, B.A. Saville, *Introduction to Chemical Reaction Engineering and Kinetics*, John Wiley & Sons, Inc, Toronto, 1999.
- [28] R. Liu, R. Tsiava, S. Xu, D. Chen, Experimental study of char gasification characteristics with high temperature flue gas, *J. Energy Inst.* vol. 97 (April) (2021) 187–193, <https://doi.org/10.1016/j.joei.2021.04.015>.
- [29] M. Baerns, et al., *Technische Chemie, 1. Edition*, WILEY-VCH, Weinheim, 2006.
- [30] C.E. Agu, C. Pfeifer, B.M.E. Moldestad, Prediction of void fraction and minimum fluidization velocity of a binary mixture of particles: bed material and fuel particles, *Powder Technol.* vol. 349 (2019) 99–107, <https://doi.org/10.1016/j.powtec.2019.03.027>.
- [31] C.E. Agu, L.A. Tokheim, C. Pfeifer, B.M.E. Moldestad, Behaviour of biomass particles in a bubbling fluidized bed: a comparison between wood pellets and wood chips, *Chem. Eng. J.* vol. 363 (November 2018) (2019) 84–98, <https://doi.org/10.1016/j.cej.2019.01.120>.
- [32] S. Gupta, S. Choudhary, S. Kumar, S. De, Large eddy simulation of biomass gasification in a bubbling fluidized bed based on the multiphase particle-in-cell method, *Renew. Energy* vol. 163 (2021) 1455–1466, <https://doi.org/10.1016/j.renene.2020.07.127>.
- [33] J.J. Hernández, G. Aranda-Almansa, A. Bula, Gasification of biomass wastes in an entrained flow gasifier: effect of the particle size and the residence time, *Fuel Process. Technol.* vol. 91 (6) (2010) 681–692, <https://doi.org/10.1016/j.fuproc.2010.01.018>.
- [34] F.S. Char-co, G. Kinetics, I. Studies, Flax straw char-CO₂ gasification kinetics and its inhibition studies with CO, *Can. J. Chem. Eng.* vol. 91 (May) (2013) 882–888, <https://doi.org/10.1002/cjce.21696>.
- [35] A. Gómez-Barea, P. Ollero, C. Fernández-Baco, Diffusional effects in CO₂ gasification experiments with single biomass char particles. 1. experimental investigation, *Energy Fuels* vol. 20 (5) (2006) 2202–2210, <https://doi.org/10.1021/ef050365a>.
- [36] R. Bilbao, J. Lezaun, M. Menéndez, J.C. Abanades, Model of mixing-segregation for straw/sand mixtures in fluidized beds, *Fuel Process. Technol.* vol. 56 (3) (1988) 149–155, [https://doi.org/10.1016/0032-5910\(88\)80026-3](https://doi.org/10.1016/0032-5910(88)80026-3).
- [37] B. Cluet, G. Mauviel, Y. Rogaume, O. Authier, A. Delebarre, Segregation of wood particles in a bubbling fluidized bed, *Fuel Process. Technol.* vol. 133 (2015) 80–88, <https://doi.org/10.1016/j.fuproc.2014.12.045>.
- [38] L. Xiaodong, Y. Jianhua, N. Mingjiang, C. Kefa, Study on mixing performance of municipal solid waste (MSW) in differential density fluidized beds (FBs), *Chem. Eng. J.* vol. 84 (2) (2001) 161–166.
- [39] Q. Wang, et al., Application of CPFD method in the simulation of a circulating fluidized bed with a loop seal Part II-Investigation of solids circulation, *Powder Technol.* vol. 253 (2014) 822–828, <https://doi.org/10.1016/j.powtec.2013.11.040>.
- [40] X. Jing, et al., Evaluation of CO₂ gasification reactivity of different coal rank chars by physicochemical properties, *Energy Fuels* vol. 27 (12) (2013) 7287–7293, <https://doi.org/10.1021/ef401639v>.
- [41] X. Yao, Q. Yu, Z. Han, H. Xie, W. Duan, Q. Qin, Kinetics of CO₂ gasification of biomass char in granulated blast furnace slag, *Int. J. Hydrog. Energy* vol. 43 (27) (2018) 12002–12012, <https://doi.org/10.1016/j.ijhydene.2018.04.102>.
- [42] P. Lahijani, Z.A. Zainal, A.R. Mohamed, M. Mohammadi, Microwave-enhanced CO₂ gasification of oil palm shell char, *Bioresour. Technol.* vol. 158 (2014) 193–200, <https://doi.org/10.1016/j.biortech.2014.02.015>.
- [43] S. Pratschner, M. Hammerschmid, S. Müller, F. Winter, Evaluation of CO₂ sources for power-to-liquid plants producing Fischer-Tropsch products, *J. CO₂ Util.* vol. 72 (May) (2023) 102508, <https://doi.org/10.1016/j.jcou.2023.102508>.

- [44] D. Kunii, O. Levenspiel, *Fluidization Engineering*, vol. 74, Butterworth-Heinemann, Boston, London, Singapore, Sydney, Toronto, Wellington, 1991, <https://doi.org/10.1016/C2009-0-24190-0>.
- [45] F. Scala, R. Chirone, P. Salatino, Combustion and attrition of biomass chars in a fluidized bed, *Energy Fuels* vol. 20 (1) (2006) 91–102, <https://doi.org/10.1021/ef050102g>.
- [46] P. Weerachanchai, M. Horio, C. Tangsathikulchai, Effects of gasifying conditions and bed materials on fluidized bed steam gasification of wood biomass, *Bioresour. Technol.* vol. 100 (3) (2009) 1419–1427, <https://doi.org/10.1016/j.biortech.2008.08.002>.
- [47] A.M. Mauerhofer, J.C. Schmid, F. Benedikt, J. Fuchs, S. Müller, H. Hofbauer, Dual fluidized bed steam gasification: change of product gas quality along the reactor height, *Energy* vol. 173 (2019) 1256–1272, <https://doi.org/10.1016/j.energy.2019.02.025>.
- [48] J.R. Grace, *Contacting modes and behaviour classification of gas-solid and other two-phase suspensions*, *Can. J. Chem. Eng.* vol. 64 (June) (1986) 353–363.
- [49] C.Y. Wen, Y.H. Yu, A generalized method for predicting the minimum fluidization velocity, *Am. Inst. Chem. Eng. J.* vol. 12 (3) (1966) 610–612, <https://doi.org/10.1002/aic.690120343>.
- [50] A. Fenghour, W.A. Wakeham, V. Vesovic, The viscosity of carbon dioxide, *J. Phys. Chem. Ref. Data* vol. 27 (1) (1998) 31–39, <https://doi.org/10.1063/1.556013>.